A&A 542, A56 (2012)
DOI: 10.1051/0004-6361/201117844

Astronomy & Astrophysics

Accretion flow dynamics during the evolution of timing and spectral properties of GX 339-4 during its 2010–11 outburst⋆

A. Nandi[1,2], D. Debnath[2], S. Mandal[3], and S. K. Chakrabarti[4,2]

[1] Space Astronomy Group, ISRO Satellite Centre, HAL Airport Road, 560017 Bangalore, India
e-mail: anuj@isac.gov.in
[2] Indian Centre for Space Physics, Chalantika 43, Garia Station Rd., 700084 Kolkata, India
e-mail: dipak@csp.res.in
[3] Indian Institute of Space Science and Technology, 695547 Thiruvananthapuram, India
e-mail: samir@iist.ac.in
[4] S. N. Bose National Centre for Basic Sciences, Salt Lake, 700098 Kolkata, India
e-mail: chakraba@bose.res.in

Received 7 August 2011 / Accepted 28 March 2012

ABSTRACT

Context. The Galactic transient black hole candidate (BHC) GX 339-4 exhibited several outbursts at regular intervals of about two to three years in the *Rossi* X-ray Timing Explorer (RXTE) era. After remaining in an almost quiescent state for three long years, it again became X-ray active in January, 2010, continuing to be so over the next ∼14 months.
Aims. We study the timing and spectral properties of the BHC during its recent outburst and understand the behavioral change in the accretion flow dynamics associated with the evolution of the various X-ray features.
Methods. The detailed analysis of the temporal and spectral properties of the source during this outburst are carried out using archival data of the RXTE PCA instrument. We analyze a total of 236 observational intervals consisting of 419 days of data observed by RXTE, from 2010 January 12 to 2011 March 6.
Results. Our study provides a comprehensive understanding of the mass accretion processes and properties of the accretion disk of the BHC. The PCA spectra of 2.5–25 keV are mainly fitted with a combination of two components, namely, a disk black body and a power-law. The entire outburst as observed by RXTE, is divided into four spectral states, namely, hard, hard-intermediate, soft-intermediate, and soft. Quasi-periodic oscillations (QPOs) were found in three out of the four states, namely hard, hard-intermediate, and soft-intermediate states. The QPO frequencies increase monotonically from 0.102 Hz to 5.692 Hz in the rising phase of the outburst, while during the declining phase QPO frequencies decrease monotonically from 6.420 to 1.149 Hz. The evolution pattern, i.e. the hardness-intensity diagram, of the present outburst can be reproduced by two different components of the flow of accreting material.
Conclusions. The recent outburst of GX 339-4 gives us an opportunity to understand the evolution of the two-component accretion rates starting from the onset to the end of the outburst phase. We found that the QPO frequency variation could be explained by the propagating oscillatory shock model (POS) and the hardness versus intensity variation can be reproduced if we assume that higher viscosity causes the conversion of a low angular momentum disk component into a Keplerian component during the outburst phase. The decline phase starts because of the reduction in the viscosity.

Key words. stars: individual: GX 339-4 – X-rays: binaries – accretion, accretion disks – black hole physics – shock waves

1. Introduction

The Galactic transient black hole (BH) candidates are the most interesting X-ray objects to study, as these sources undergo peculiar temporal and spectral changes during their outburst phases. Several spectral states are identified in BH outburst sources based on the evolution of their spectral and timing properties (McClintock & Remillard 2006; Belloni et al. 2005; Remillard & McClintock 2006). The spectral evolution of states in BH transients are also found to be associated with different branches of a q-like pattern (hysteresis loop), which is an X-ray hardness-intensity diagram (HID) (Maccarone & Coppi 2003; Homan & Belloni 2005) in the log-log plot. The existence of the similar loop feature is also reported for the neutron star binaries (Maccarone & Coppi 2003) as well as for the cataclysmic variables (CVs) (Kording et al. 2008). In general, during an outburst, the spectral states are identified as four basic states – *hard, hard-intermediate, soft-intermediate*, and *soft* states. One can find extensive discussions in the literature of the basic properties of all these four states (Homan & Belloni 2005; Debnath et al. 2008; Motta et al. 2009; Dunn et al. 2010). In addition, a different state, termed the *very high* state, is also observed corresponding to the highest luminosity of some of the outburst sources (see Miyamoto et al. 1991; Remillard et al. 1999).

The temporal analysis of the X-ray variabilities observed in the outburst sources also reveals a unique type of evolution in the power density spectrum (PDS). The PDSs are composed of different type of components, such as a flat-top (white noise) component, a break frequency (zero-centered Lorentzian function), and a power-law like distribution (red noise) etc. with a low-to-intermediate quasi-periodic oscillations (QPOs) (<20 Hz) (Belloni et al. 2002a; Titarchuk et al. 2007). The observed QPOs are classified into three different classes "A", "B",

⋆ Tables A.1–A.3 are only available at the CDS via anonymous ftp to cdsarc.u-strasbg.fr (130.79.128.5) or via http://cdsarc.u-strasbg.fr/viz-bin/qcat?J/A+A/542/A56

and "C" types (see for details, Wijnands et al. 1999; Homan et al. 2001; Remillard et al. 2002), mostly based on the coherence factor Q ($=\nu/\Delta\nu$, where ν is the centroid frequency of QPO and $\Delta\nu$ is the FWHM) and the presence of the weak/strong noise component in the power spectra.

GX 339-4 is a well-studied transient stellar-mass black-hole binary having a mass function of $M = 5.8 \pm 0.5\ M_{\odot}$ (Hynes et al. 2003) and a low-mass companion of mass 0.52 $M_{\odot}$ and being located at a distance $d \geq 6$ kpc (Hynes et al. 2003, 2004). The inclination angle (i) of the system has not yet been confirmed. Zdziarski et al. (2004) indicated the lower limit of $i \geq 45°$, while Cowley et al. (2002) indicated the upper limit of $i \leq 60°$, although there is another report of an inclination angle of $i \sim 20°$ (Miller et al. 2004) of this source.

GX 339-4 has undergone several outburst phases (Nowak et al. 1999; Belloni et al. 2005; Motta et al. 2009; Debnath et al. 2010) during the *Rossi* X-ray Timing Explorer (RXTE) era (in the period from 1998 to 2011). Since its discovery (Markert et al. 1973), the source has been found to be in low luminosity (quiescent state) states, although there have been several reports of state transitions (Maejima et al. 1984; Ilovaisky et al. 1986). As for other transient black-hole candidates (e.g., GRO J1655-40, XTE J1550-564, H 1743-322), the complex outburst profile of the source, generally, begins and ends in the low-hard state (Belloni et al. 2005; Debnath et al. 2008).

This general behavior of the outburst profile can be explained using a two-component advective flow model (Chakrabarti & Titarchuk 1995, hereafter CT95) having a standard Shakura-Sunyaev Keplerian disk (Shakura & Sunyaev 1973) on the equatorial plane and a sub-Keplerian (low angular momentum) accreting halo on top of the Keplerian disk. The sub-Keplerian halo in the shocked-accretion phase produces the Compton cloud (inner part of the disk) of hot electrons, while the Keplerian disk produces the soft photons. The high energy part of the spectrum is due to the inverse Comptonization of the soft photons by the hot electrons supplied by the sub-Keplerian disk. In this scenario, the outburst phenomenon could be due to a sudden increase in the viscosity of the accretion-disk system (e.g., Frank et al. 2002). More specifically, Mandal & Chakrabarti (2010) suggests that the enhanced viscosity converts part of the sub-Keplerian matter (i.e., low angular momentum flow) into a viscous Keplerian flow (i.e., matter in Keplerian rotation), keeping the total mass-flow rate roughly constant. The sudden increase in the accretion rate of the Keplerian matter and its inward movement cause the sudden enhancement of luminosity. The declining phase starts when the source of the enhanced viscosity is removed and there is a shortfall of the Keplerian component.

The typical evolution of the QPOs during the outburst phases of the transient black-hole sources has been well-established for a long time (Belloni & Hasinger 1990; Belloni et al. 2002a; Belloni et al. 2005; Debnath et al. 2008, 2010, 2012; Chakrabarti et al. 2005, 2008, 2009). The outbursting BHCs in general show signatures of low and intermediate frequency QPOs during the initial rising phase (mainly low-hard state) as well as in the decline phase of the outburst, where the sub-Keplerian rate dominates and during the intermediate state, where the Keplerian and sub-Keplerian rates are more or less comparable to each other. In general, during the rising phase (hard state) of the outburst, the frequency of the QPO increases, whereas during the declining phase, the QPO frequency gradually decreases. These QPO types of evolution (increasing/decreasing nature of QPO frequencies) in these objects can be well-understood due to the propagating oscillatory shocks (POS; Chakrabarti et al. 2008, 2009; Debnath et al. 2010) model.

After remaining in the "quiescent" state for almost three years (the last outburst took place during the year 2006/2007, although there is report of weak activity in 2009 as observed by *Swift*/BAT), GX 339-4 showed X-ray flux activity of 17 mCrab (4–10 keV) on January 03, 2010 with the first detection by MAXI/GSC onboard ISS (Yamaoka et al. 2010). The source remained active in X-rays for the next ~430 days and during this period, the source was extensively monitored with RXTE, starting from 2010 January 12 (Tomsick 2010). In Debnath et al. (2010, hereafter, Paper I), we provided a preliminary summary of the timing and spectral properties during the rising phase of this outburst.

In this present paper, we provide the timing and spectral results of RXTE PCA for a total of 236 observational intervals of 419 days of data, from 2010 January 12 to 2011 March 6. From our study, a comprehensive understanding of the mass accretion processes and properties of the accretion disk of this BHC has emerged. The PCA spectra of 2.5–25 keV were mainly fitted with the combination of two components of a disk black body and a power law whereas the soft state spectra were fitted across the energy range of 2.5–10 keV (few spectra extended up to 15 keV also) because of very low and insignificant flux contributions above 10 keV. On the basis of the relative importance of the black body and the power-law components, the outburst is divided into four spectral states, namely, *hard, hard-intermediate, soft-intermediate*, and *soft* (Homan & Belloni 2005), in the sequence of *hard* → *hard-intermediate* → *soft-intermediate* → *soft* → *soft-intermediate* → *hard-intermediate* → *hard*. Since the definitions vary, we here define the hard state to be the one in which the temperature ($T_{\rm in}$) and photon index (Γ) parameters have values greater than ~1.5 keV and less than ~1.6 respectively, whereas in the hard-intermediate state (i.e., in rising and declining phases) the parameters vary rapidly within the ranges of ~1.5–1.0 keV and ~1.6–2.3. In the soft-intermediate state, the $T_{\rm in}$ and Γ parameters have values within the range of ~0.9–0.7 keV and ~2.3–2.5, whereas in the soft state the values are <0.7 keV and ~3.0, respectively. Debnath et al. (2012) also reported the similar and cyclic order of state transitions in the 2010 and 2011 outbursts of the transient Galactic black-hole candidate H 1743-322. The temporal variations in these states and state transitions are also found to be unique and tightly correlated with the spectral properties.

The paper is organized in the following way: In the next section, we discuss the observations and data analysis procedures using HEASoft software. In Sect. 3, we present the details of our temporal and spectral analysis of PCA data and discuss possible accretion-disk flow behavior during the outburst phase. Finally, in Sect. 4, we present a brief discussion of our results and provide some concluding remarks.

2. Observation and data analysis

We present our analysis of publicly available archival data from the RXTE Proportional Counter Array (PCA) instrument of the entire 2010-11 outburst of GX 339-4. We extracted and analyzed the RXTE archival data from 2010 January 12 (modified Julian date (MJD) 55208) to 2011 March 6 (MJD 55626) from the PCA (Jahoda et al. 1996). We extracted light curves and PDS for different energy bands and the energy spectra from the good and the most reliably calibrated detector units i.e., PCU2, for the PCA. We also analyzed RXTE/ASM data to have a quick look at the outburst profile. The results of our analysis using the ASM data were published in Debnath et al. (2010). Here, we

only present results based on the analysis of the archival data of the PCA instrument.

We carry out our data analysis using the FTOOLS software package HeaSoft version HEADAS-6.10 and XSPEC version 12.6. For the timing analysis, we use the science data of the *Event mode* (*E_125us_64M_0_1s*, FS37*.gz) with a maximum time resolution of 125 μs. We use standard FTOOLS tasks ("xtefilt", "maketime") to generate both a filter file using the latest pca breakdown history file and a good time interval (gti) file for PCU2. To determine the "good time interval" for each observation, we use the screening criteria of elevation angle >10°, offset <0.02°, SAA passage time (within 30 min of passage), and HV breakdown time for the PCU2 detector only. Light curves were extracted using the "sefilter" and "saextrct" task for the event and science data, respectively.

For spectral analysis, *Standard2* mode Science Data of PCA (FS4a*.gz) are used. Spectra are extracted from all the layers of the PCU2 for 128 channels (without any binning/grouping the channels). We exclude the HEXTE data from our analysis, as we find strong residuals (line features) in the HEXTE spectra at different energies. This is possibly due to the difficulties in estimating the background spectra as the "rocking" mechanism has stopped functioning for HEXTE. So, we restrict our spectral analysis for the PCA data for energy range of 2.5–25 keV, although we analyzed the PCA spectral data in a few observations (for energies up to 40 keV) to search for the high energy contribution to the low-hard states. The "runpcabackest" task was used to estimate the PCA background using the latest bright-source background model (count rates were always high, except for the last few observations of the decline phase, where the net count rates per PCU were ≤40 counts/s). We also incorporated the *pca_saa_history* file to take care of the SAA data. To generate the response files, we used the "pcarsp" task. In general, we follow the same analysis techniques discussed in Paper I (Debnath et al. 2010) for the timing and spectral analysis purposes.

3. Results and modeling

The study of the X-ray temporal and spectral properties of compact objects, specially for outbursting BHCs, is essential to determine the flow properties during the outburst phases of the sources. It was pointed out by Debnath et al. (2010) that there are two main types of outbursting BHCs, one of so-called type fast-rise slow-decay (FRSD) and another of slow-rise slow-decay (SRSD) (i.e., GX 339-4), although the general behavior of outbursting X-ray binaries is far more complex. Chen et al. (1997) carried out an extensive study of the light curve morphology of several X-ray binaries and classified them into five morphological types. To study the X-ray intensity variations of the 2010 outburst of GX 339-4, we extracted light curves from PCU2 data acquired by the RXTE/PCA instrument in the different energy bands 2–6 keV (5–13 ch.), 6–20 keV (14–46 ch.), and 2–20 keV (5–46 ch.). We divided the 2–20 keV energy band into the above two bands because the 2–6 keV photons mainly come from a thermally cool Keplerian disk, whereas the photons in the higher energy band (6–20 keV) band come from a Comptonized sub-Keplerian disk (Compton corona).

In Figs. 1a, b, the total 2–20 keV PCU2 light curve (counts/sec) and the hardness ratio (ratio of the photon count rates in the 6–20 keV to 2–6 keV bands) are plotted. The origin of the time axis is MJD 53 200 (2010 January 4), which is eight days prior to our first observation. The hardness ratio variation distinctly reflects the indication of spectral state transitions. The hard to hard-intermediate state transition took place

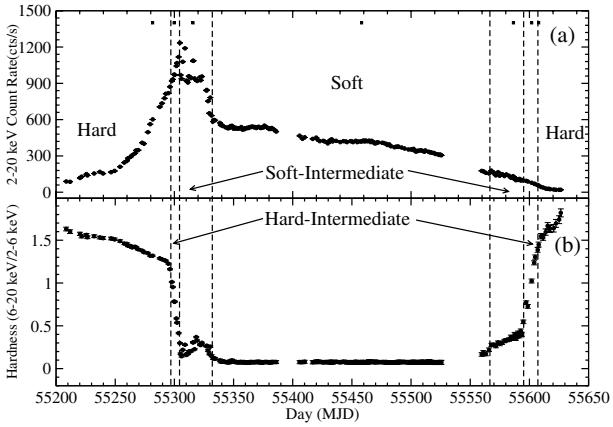

Fig. 1. a) 2–20 keV PCA light curve and **b)** hardness ratio (6–20 keV versus 2–6 keV count ratio) as a function of the MJD of the event (i.e., 2010–11 outburst of GX 339-4). The vertical dashed lines indicate the transition of states and filled squared points in **a)** are the seven observed days from seven different spectral states, whose detailed timing and spectral results are discussed in this paper.

on 2010 April 10 (MJD 55 296), the hard-intermediate to soft-intermediate transition on 2010 April 18 (MJD 55 304), the soft-intermediate to soft transition on 2010 May 15 (MJD 55 331), the reverse transition from the soft to soft-intermediate state on 2011 January 4 (MJD 55 565), the soft-intermediate to hard-intermediate state transition on 2011 February 2 (MJD 55 594), and finally on 2011 February 14 (MJD 55 606) the state transition from hard-intermediate to hard state occurred. These are indicated by vertical dotted lines in the plot of Fig. 1. It is observed that rapid changes in the hardness ratio occur only in the hard and hard-intermediate states, whereas in the soft and soft-intermediate states the hardness ratio changes only very slowly. Both the rising and falling arms of the outburst profile correspond to the hard state and in both the cases, we found evidence of strong QPOs. However, the local changes in the temporal and spectral features in different states cannot be discerned from this plot. This leads us to conduct a thorough and robust temporal and spectral analysis using the PCA data and the results are presented in the following sections.

The source was in a hard state from our initial RXTE/PCA observation day (2010 January 12, MJD 55 208) to 2010 April 9 (MJD 55 295). During this initial rising phase, no QPOs were detected until 2010 March 21. On 2010 March 22, for the first time a QPO of 102 mHz frequency was observed. After that, it increased monotonically until 2010 April 17, when we observed a QPO of 5.692 Hz. The source moved to a hard-intermediate spectral state on 2010 April 10 (MJD 55 296), where it remained until 2010 April 17 (MJD 55 303). On 2010 April 18 (MJD 55 304), the source moved to a soft-intermediate spectral state and remained in this state until 2010 May 14 (MJD 55 330). During this spectral state, QPOs were observed sporadically on and off at ∼6 Hz. After that on 2010 May 15 (MJD 55 331), the source moved to a soft spectral state, during which no QPO was observed. It remained in this state for around next seven and a half months, until 2011 January 3 (MJD 55 564). During this time, it emitted a hard X-ray flux (>10 keV) dominated by a sub-Keplerian flow component that diminished rapidly with time to produce spectral data of too low signal-to-noise ratio above ∼15 keV. On 2011 January 4 (MJD 55 565), the source underwent a spectral transition to the soft-intermediate state as the flux became increasingly hard. During this spectral state, sporadic QPOs of frequency ∼2 Hz were observed, as in the same state

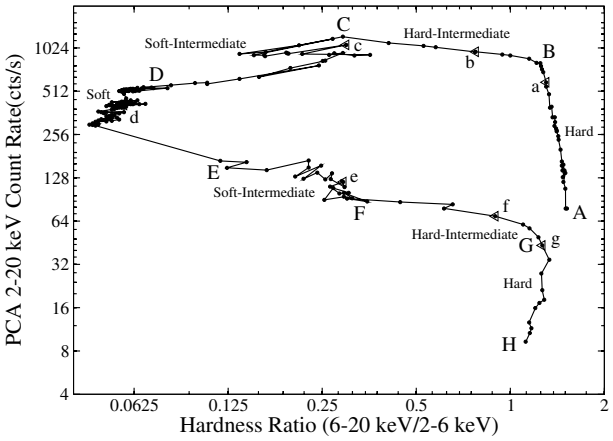

Fig. 2. Hardness intensity diagram of GX 339-4 in the 2010-11 outburst observed with RXTE/PCA. We have plotted the total count rates in 2–20 keV energy band along *Y*-axis and the ratio of the count rates in the 6–20 keV to 2–6 keV bands along the X-axis. The points *A*, *B*, *C*, *D*, *E*, *F*, *G*, and *H* are observations on MJD 55 208, MJD 55 296, MJD 55 304, MJD 55 331, MJD 55 565, MJD 55 594, MJD 55 606, and MJD 55 626, respectively, which indicate the start/state transitions/end of our observation. In addition, the points *a*, *b*, *c*, *d*, *e*, *f*, and *g* (marked with triangle on plot) are the seven observed points from seven different states, whose detailed timing and spectral results are discussed in this paper. Note that the *X* and *Y* axes are on logarithmic scales.

Table 1. Temporal properties of power spectra in different states.

Obs. (1)	ν (2)	$\Delta\nu$ (3)	Q (4)	Type (5)	$\nu_{\rm brk}$ (6)	Noise/Comp. (7)	rms(%) (8)	χ^2/d.o.f. (9)
26	$0.134^{+0.006}_{-0.006}$	$0.022^{+0.001}_{-0.002}$	6.091	C	0.88	lo + lo + lo	36%	77.76/81
	$2.423^{+0.006}_{-0.006}$	$0.072^{+0.006}_{-0.007}$	33.65	C	0.44			
35	$4.853^{+0.029}_{-0.036}$	$0.412^{+0.127}_{-0.120}$	11.78	C	...	lo+lo+lo+lo+lo	19%	108.64/76
	$7.249^{+0.122}_{-0.137}$	$1.256^{+0.724}_{-0.446}$	5.771	C	...			
51	$5.908^{+0.038}_{-0.037}$	$1.021^{+0.086}_{-0.083}$	5.786	B	2.122	po+lo+lo+lo	11%	113.9/79
141	...	...	...	...	...	po	3%	96.39/88
208	$2.136^{+0.138}_{-0.160}$	$1.065^{+0.087}_{-0.068}$	2.005	B	...	po+lo	11%	77.17/85
222	$1.322^{+0.002}_{-0.024}$	$0.162^{+0.053}_{-0.056}$	8.160	C	0.331	lo+lo+lo	23%	73.73/81
226	...	...	...	...	0.133	lo+lo	24%	92.14/84

Notes. The rms is calculated for each power spectra from 0.01 to 20 Hz.

of the initial rising phase. After this time, the source returned to a hard-intermediate state on 2011 February 2 (MJD 55 594). During this phase, QPOs of monotonically decreasing frequency were observed, as for other transient BHCs (e.g., the 2005 outburst of transient Galactic BHC GRO J1655-40; Chakrabarti et al. 2008; Debnath et al. 2008, and the 2010 and 2011 outbursts of H 1743-322; Debnath et al. 2012). After that, the source returned to its hard state on 2011 February 14 (MJD 55 606). Here we should also observe QPO evolutions. However, owing to decreases in their photon fluxes and a lack of long duration observations, low-frequency QPOs have not been detected prominently, only break frequencies being observed (see, Table 1).

To clearly monitor the evolution of states during the outburst, we need to draw the HID and study the evolution of timing and spectral properties during different branches of the HID. In Fig. 2, we plot the PCA 2–20 keV count rate of the 2010−11 outburst against X-ray color (PCA count ratio of the flux in the 6–20 keV to that in the 2–6 keV energy band). The points *A* and *H* are the indicators of the start and the end of the RXTE observations respectively, whereas the points *B*, *C*, *D*, *E*, *F*, and *G* are the points on the days where the state transitions occurred.

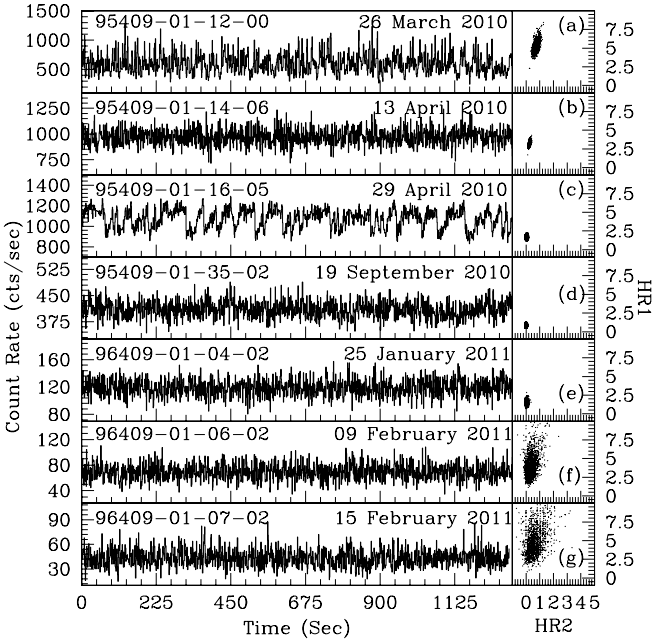

Fig. 3. a–g) In each plot, we plot in the left panel the 2–25 keV PCA light curve and in the right panel the color–color diagram are plotted. These plots **a–g)** are associated with MJD 55 281, MJD 55 299, MJD 55 315, MJD 55 458, MJD 55 586, MJD 55 601, and MJD 55 607, respectively and represent seven different spectral states of the outburst of GX 339-4.

In Figs. 3a–g, we plotted the light curves and color–color diagrams for seven data sets (a–g, marked in Fig. 2) to study the X-ray variability and hardness ratio variation in different branches of the HID. We extracted PCA light curves for the above seven data sets using time bins of 1 s in three different energy channels: *I* consisting of 5–8 channels (2–4 keV), *II* of 9–35 channels (4–15 keV), and *III* of 36–58 channels (15–25 keV). Using these light curves, we generated a total light curve for the 2–25 keV energy range and two X-ray colors defined as HR2 (*III*/*I*) versus HR1 (*II*/*I*). Light curves were then background subtracted. The spectral data shows that the background rates are ∼10 to 15 cts/sec in the energy range of 2–25 keV. Our motivation for splitting the energies in to the above mentioned intervals was to separate the contributions of photons coming from the Keplerian and sub-Keplerian disk components. The photons from the Keplerian disk are emitted primarily at low energies (<∼4 keV), whereas the same from the sub-Keplerian flow were emitted at higher energies (>∼4 keV) for the stellar-mass black-hole candidates. Thus, *I* is emitted mostly from the Keplerian component, whereas the component *II* might be emitted from the region where the moderate thermal Comptonization of the Keplerian photons take place. The component *III* should be emitted from the region that is definitely depleted or enhanced during state transitions as it represents the higher energy side of the pivotal energy [∼15 keV] in the spectrum. Thus, these figures carry some information about the disk geometry, i.e., the number of soft photons produced by the Keplerian disk (∼*I*) and the number of Comptonized photons that produced by the "Compton cloud" [∼(*II* + *III*)].

Figures 3a–d represent the hard, hard-intermediate, soft-intermediate, and soft states, respectively, of the rising phase of the outburst. The corresponding color-color diagrams show that the photon intensity of the harder component (*III*) is strongest

in the hard state and slowly decreases as the outburst moves to a soft state. However, the soft component (*I*) has the opposite behavior, namely it brightens and emits its strongest flux in the soft state. The photon intensities of bands *III* and *I* are comparable to each other the in hard-intermediate state. The PDS of this hard state data shows a strong signature of a QPO at 0.134 Hz, whereas that of the hard-intermediate state shows a QPO at 2.423 Hz with harmonics at 4.853 Hz and 7.249 Hz.

A B-type QPO of frequency ∼6 Hz is observed in the soft-intermediate state. Interestingly, we observe variability of longer timescale (few tens of seconds) for some obs-IDs in the soft-intermediate state. A similar kind of variability was also observed in the very high state (VHS) of GX 339-4 with timescales of 20 to 60 s (Miyamoto et al. 1991). The dynamic nature of this type of variability will be studied in detail and presented elsewhere. In the soft state, the sub-Keplerian disk becomes cooler, a greater supply of Keplerian matter, and we observe no signatures of QPOs.

Figures 3e–g again shows the soft-intermediate, hard-intermediate, and hard spectral state, respectively, but in the declining phase of the outburst. From the color-color variations, we note that the soft-photon intensity (*I*) decreases and the hard component of the flow (*III*) becomes stronger. The soft-intermediate data shows a QPO of frequency 2.136 Hz. The hard-intermediate and hard states display similar variations to the same states in the rising phase of the outburst, except that the X-ray intensities (counts/sec) in different energy bands are somewhat weaker. A strong QPO of 1.322 Hz was observed in the hard-intermediate state, whereas in the hard state a weak QPO of break frequency type was observed (see Table 1 for details).

In the subsequent subsections, we present the modeling of the power spectral evolution, the QPO characteristics during the outburst phase, and the spectral energy distribution. The detailed temporal and spectral analysis results of the entire observation are tabulated in online tables (Tables A.1–A.3).

3.1. Power density spectra

In Sect. 3, we have examined the PCA light curves and color variations in different branches of the HID. This motivated us to carry out a similar type of examination in power spectra in each data set to obtain a clearer picture of the disk dynamics following the HID variations. Power spectra were produced with a time resolution of 1/2048 s (using the event mode data of 122 μs time resolution), which corresponds to a Nyquist frequency of 1024 Hz. For each observation, we fit the average spectra (energy range of 2–15 keV) with a constant to estimate the white noise component (Poissonian noise). We found that the expected white noise level (above 30 Hz) in hard states has a power of ∼1.97, whereas in soft states the level was around 2. During the PDS analysis, we did not include the dead time effects because the count rates are not so high (maximum rate around 1200 cts/s). We verified that the error caused by the PCA dead time is at most 4%. We used the "powspec" task of the XRONOS package with a normalization factor of "−2" to ensure that the expected "white" noise was subtracted from the rms fractional variability of PDS. The power has the unit of rms^2/Hz. We re-binned the power spectrum with a geometrical factor of −1.05 to have nearly equispaced logarithmic frequency bins and fitted each spectrum within the range from 0.01 to 20 Hz.

In Figs. 4a–d, we present power spectra from four different regions (labeled a, b, c, and d) of Fig. 2. The power spectra are generally dominated by flat-top (white noise) and power-law like

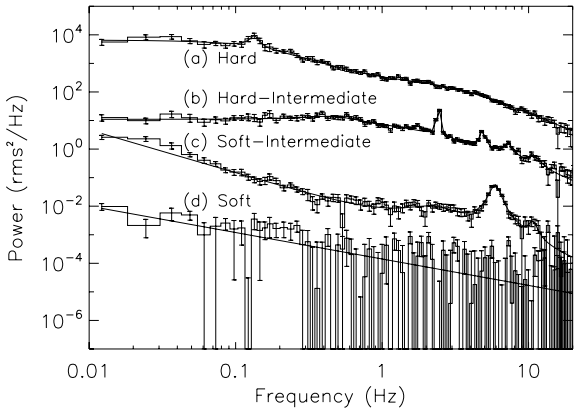

Fig. 4. Model-fitted PDS of four spectral states (a, b, c, and d in Fig. 2) are shown. From top to bottom: hard state data of 2010 March 26 (Obs. ID: 95409-01-12-00), hard-intermediate state of 2010 April 13 (Obs. ID: 95409-01-14-06), soft-intermediate state of 2010 April 29 (Obs. ID: 95409-01-16-05), and soft state of 2010 September 19 (Obs. ID: 95409-01-35-02) PDS are shown. For a clear view, the Y-scale of (a), (b), and (c) plots are multiplied by the factor of 2×10^4, 10^3, and 20, respectively.

(red noise) components, which have typically been fitted with a zero-centered Lorentzian (Belloni et al. 2002b). The presence of QPOs in the power spectra has also been fitted by a Lorentzian (Nowak 2000; van der Klis 2005). We fitted all the PDSs with either Lorentzian profiles or power-law like distributions in the frequency range from 0.01 to 20 Hz. The overall fitted results of the power spectra along with the best-fit parameter values for the QPOs in all four cases are given in Table 1. After fitting PDS, we used the "fit err" task to calculate the error in the QPO frequencies, widths, and powers. This task calculates the 90% confidence range of any fitted parameter.

In Fig. 4a, we present the Lorentzian-model-fitted power spectrum of the light curve of 2010 March 26 (Obs. ID: 95409-01-12-00), which belongs to the *hard* state of the HID (the *A* to *B* branch) and also contains the prominent signature of a type-C QPO. In this branch of the HID, the power spectra are generally fitted with three Lorentzians – (i) in the flat-top noise part plus a power-law distribution up to the break frequency (with a zero-center Lorentzian); (ii) at QPO frequencies; and (iii) for the high-frequency power law after the break frequency. The break frequency and QPOs observed in the power spectra vary, respectively, from 0.5 to 2.0 Hz and from 0.102 Hz to 0.547 Hz as the source moves from hard to hard-intermediate states. All observations in this state are those of a strong "C" type QPO.

The model-fitted power spectra in Fig. 4b belong to the *hard-intermediate* state and were observed on 2010 April 13 (Obs. ID: 95409-01-14-06). A strong flat-top noise component along with a characteristic break frequency at 0.44 Hz and QPO frequency around 2.42 Hz with harmonics are discernible in the PDSs, which in this branch of the HID (*B* to *C*) are also fitted with the same Lorentzian components as in the previous observations. The QPOs observed in this branch are of type-C and the QPO frequency increased as the source moved towards the soft-intermediate state. We observe that the flat-top noise component diminished and the power-law like distribution started to dominate the power density spectra in the low frequency range as the source moved towards the soft-intermediate state.

In Fig. 4c, we present the model-fitted PDS for observation performed on 2010 April 29 (Obs. ID: 95409-01-16-05), which corresponds to a *soft-intermediate* state. A strong QPO of type-B is observed in the PDS. The PDSs are generally fitted

with power-law and Lorentzian-type profiles. In this branch of the HID (from *C* to *D*), the QPOs are observed sporadically at around 6 Hz.

In Fig. 4d, we present the power spectra of the observation on 2010 September 19 (Obs. ID: 95409-01-35-02), which belongs to the *soft* state of the HID (*D* to *E*). In the soft states, no QPOs were observed and the power spectra were mostly dominated by a single power-law like distribution of slope ∼−1.

The power spectra in the bottom branch of the HID (*E* to *F*, *F* to *G*, and *G* to *H*) belong to the soft-intermediate, hard-intermediate, and hard state of the decline phase, which have the same features as previous observations in the top branches (*D* to *C*, *B* to *C*, and *A* to *B*) of the HID, but with less variability as the photon count rate (see, Fig. 2) has decreased significantly. The model-fitted parameters and calculated rms power of all of these three states are given in Table 1.

The evolution of broad aspects of the power spectra in different states could be well-understood by studying the diffusive propagation of the perturbation in the disk-like configuration (by treating a Keplerian disk as an extended disk and a sub-Keplerian Compton cloud as an inner disk) (Shakura & Suyanev 1973; CT95; Titarchuk et al. 2007, hereafter TSA07). TSA07 showed that the entire power spectra can be modeled with a "white-red-noise" (WRN) continuum, which has two components – a low-frequency (LF) power-law like distribution and a high-frequency (HF) flat-top (white noise) along with a red-noise (power-law type) component. The HF-WRN continuum is characteristic of the hard state, whereas the LF-WRN continuum represents the soft state. In Fig. 4, the power spectra of the hard and hard-intermediate states are well-described by the HF-WRN continuum and the soft state spectra are only modeled by LF WRN (power-law) continuum. The soft-intermediate power spectra are composed of both LF and HF-WRN components. The detailed modeling of the power spectra of this source is beyond the scope of the present work.

3.2. QPO evolution and the POS model-fitted results

The evolution of the low and intermediate QPOs in the outburst sources has been reported quite extensively in the literature (Belloni & Hasinger 1990; Belloni et al. 2002a; Belloni et al. 2005; Debnath et al. 2008, 2010, 2012; Chakrabarti et al. 2005, 2008, 2009). It has been shown for several outburst sources (namely BHs) that the evolution of QPOs can be well-explained by the theoretical propagating oscillatory shock (POS) model (for details, see Chakrabarti et al. 2008, 2009; Debnath et al. 2010, 2012).

We found that our detailed PDS analysis detected QPOs in a total of 28 observations performed over in 27 days during the rising phase and in a total of 22 observations performed over 22 days during the declining phase of the outburst. Figure 5 shows the variation in the day-wise QPO frequencies i.e. QPO evolutions during (a) the initial rising phase and (b) the final declining phase of the recent GX 339-4 outburst. In both cases, these QPO evolutions are fitted with a POS model. According to this model (POS; Chakrabarti et al. 2008, 2009; Debnath et al. 2010, 2012), we can derive from the observed QPO frequency ($\nu_{\rm QPO}$) an idea about the location of the shock wave ($r_{\rm s}$), as these shock oscillations are believed to be responsible for the generation of the QPOs. The QPO frequency ($\nu_{\rm QPO}$) is proportional to the inverse of the light crossing time ($t_{\rm infall}$) from the shock location to the black-hole, i.e., $\nu_{\rm QPO} \sim (t_{\rm infall})^{-1}$ and also $t_{\rm infall} \sim R\, r_{\rm s}\, (r_{\rm s}-1)^{1/2} \sim r_{\rm s}^{3/2}$, where R is the shock compression

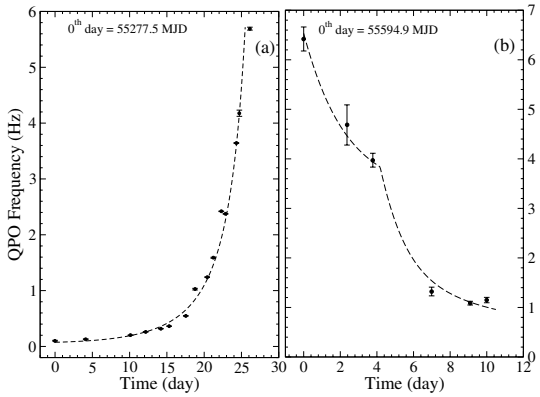

Fig. 5. Variation of the QPO frequencies with time (in day) during **a)** the rising and **b)** the declining phases of the outburst. The dotted curves are the solutions from the oscillating and propagating shocks. While in **a)**, the shock appears to be drifting at a constant speed (∼10 m s^{-1}) towards the black hole, in **b)**, the shock moves away from the black hole in two different ways. During the initial ∼4.2 days, the shock moved away with a slow rate of acceleration (∼20 cm s^{-1} day^{-1}), after which it moved away with a high acceleration (∼175 cm s^{-1} day^{-1}).

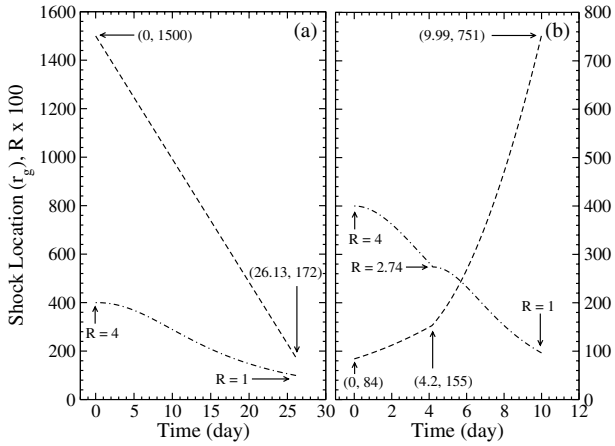

Fig. 6. Variation in the shock locations (dashed curve) and compression ratios R (dotted-dashed curve) with time (in days) during **a)** the rising and **b)** the declining phases of the outburst. See text, for details.

ratio (=ρ_+/ρ_-, where ρ_+ and ρ_- are the densities in the post- and the pre- shock flows). The QPO frequency in this model is $\nu_{\rm QPO} \sim r_{\rm s}^{-3/2}$. In a propagating shock scenario, $r_{\rm s} = r_{\rm s}(t)$, is the time-dependent shock location given by $r_{\rm s}(t) = r_{\rm s0} \pm vt/r_{\rm g}$, where v is the velocity of the shock wave, the "–" sign indicates the rising phase, the "+" sign represents the declining phase of the outburst, and $r_{\rm s}$ is measured in units of the Schwarzschild radius $r_{\rm g} = 2GM/c^2$ (G is the gravitational constant, M is the BH mass, and c is the velocity of light). For the constant movement of the shock wave (as in the rising phase of the recent GX 339-4 outburst) $v = v_0$ and for the accelerating case (as in the declining phase of the recent outburst) $v = v(t)$, can be defined as $v(t) = v_0 + at$, where a is the acceleration of the shock front.

Figure 6 shows the change in the shock locations during (a) the rising and (b) the declining phases of the outburst. In Fig. 6a, the variation in the compression ratio R (the inverse of the shock strength β) is also shown, which varies from 4 (the strongest possible shock) to ∼1 (the weakest possible shock) during the QPO evolving period of ∼26 days. Similarly during the declining phase of the outburst, R started from the strongest possible shock value (=4), after which it became weaker as the day progressed,

and reaching its lowest possible value ($R \sim 1$) on about the tenth day (2010 February 12, MJD 55 604), when a 1.149 Hz QPO was observed.

The details about the rising-phase QPO evolution are given in Paper I (Debnath et al. 2010), so we present a brief report here. During this phase, the shock moves towards the black hole with a constant speed of ~10 m s^{-1} from 1500 r_g on the first day that the QPO is observed (2010 March 22, MJD 55 277.5), where a 102 mHz frequency QPO was indeed observed until 172 r_g on 2010 April 17 (MJD 55 303.6), when a 5.692 Hz QPO was observed with a period of ~26 days. During this QPO evolutionary phase, the source remains in either a hard or hard-intermediate spectral state. After that, the source moved to a soft-intermediate spectral state and QPOs were observed sporadically at ~6 Hz, remaining in this state for the next ~26 days. It is found that the observed QPOs are of type-C in the hard and hard-intermediate states, whereas they are of type-B during the soft-intermediate spectral state.

During the declining phase of the outburst, the source was observed in the soft-intermediate state (from 2011 January 4, MJD 55 565 to 2011 February 1, MJD 55 593) just before the hard state, when QPOs were observed at ~2 Hz. After that, during the hard-intermediate state (from 2011 February 2, MJD 55 594 onwards), the QPO frequencies monotonically decrease from 6.42 Hz (on 2011 February 2, MJD 55 594) to 1.149 Hz (on 2011 February 12, MJD 55 604). After that, during the hard state no prominent QPOs were observed owing to the decrease in source flux and lack of long-duration observations, only break frequency type QPOs being observed. In our POS model solution, we break the present QPO evolution period of hard-intermediate state into two parts. During the initial 4.2 days, the shock moved away from the black hole from 84 r_g to 155 r_g with a slow variation in shock velocity (from 205 cm s^{-1} to 288 cm s^{-1}) and slow rate of acceleration (20 cm s^{-1} day^{-1}). After that, the shock wave receded at a higher rate of acceleration (175 cm s^{-1} day^{-1}), reaching 751 r_g on the last day (~10th day) of our POS model fit, where a 1.149 Hz QPO was observed. On the last day of the QPO evolution, the shock velocity was found to be ~1785 cm s^{-1}. As in the rising phase, during the declining phase of the QPO evolution, we started with a strong shock ($\beta = 0.25$, i.e., $R = 4$), which became weaker with time reaching its minimum possible value of $R = 1$. The compression ratio R decreased with time according to the relation $1/R \rightarrow 1/R_0 + \alpha(t_d)^2$, where R_0 is the initial compression ratio (here $R_0 = 4$), t_d is the time in days (assuming that the first observation day is the zeroth day), and α is a constant that determines how the shock (strength) becomes weaker with time. During the initial 4.2 days of the declining phase of QPO evolution, R decreased slowly from 4 to 2.74, while $\alpha = 0.0065$, and then on about the tenth day it reached ~1 for different α (=0.02).

During both the rising and the declining phases of the outburst, a similar propagation of shock waves was observed during the rising and declining phases of the 2005 GRO J1655-40 outburst (Chakrabarti et al. 2008). During the rising phase of the outburst, it was observed to have a monotonically increasing QPO frequency from 82 mHz to 17.78 Hz within a period of ~16 days with the constant movement ($v_s \sim 20$ m s^{-1}) of the shock wave towards the black hole from 1270 r_g to 59 r_g. During this QPO evolution phase, the shock compression ratio R reached its weakest possible value ($R = 1$), after achieving its strong shock value ($R = 4$). On the next day onwards, there was no detection of QPOs, hence it was concluded that there may be either no shock or a standing shock. However during the present GX 339-4 outburst in the soft-intermediate state, shocks might have stalled and oscillated randomly because QPOs were sporadically observed at ~6 Hz for the next ~26 days. This occurred when the rates of the two flows were comparable and the effects of the shock need not always be visible. On the other hand, during the declining phase of the 2005 GRO J1655-40 outburst, the shock moved away from the black hole starting from 40 r_g to 3100 r_g with a monotonically decreasing QPO frequency from 13.14 Hz to 0.34 Hz over a period of ~20 days. As for the recent GX 339-4 outburst, the shock also receded with a constant acceleration in two different ways, during the initial 4.2 days slowly and then with a rapid acceleration, the only difference being that during the declining phase of the 2005 GRO J1655-40 outburst, no QPOs were observed during the soft-intermediate state.

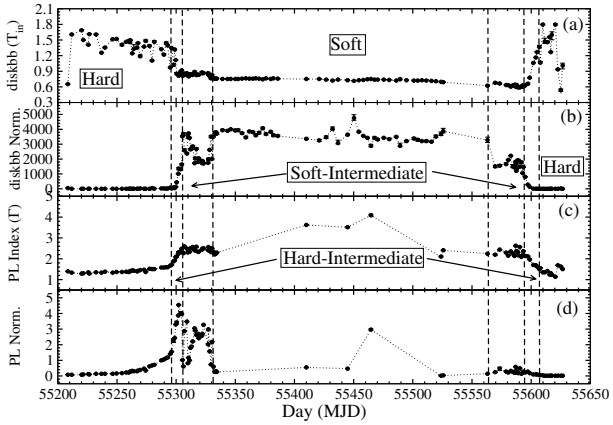

Fig. 7. Fitted model parameters of RXTE 2.5–25 keV PCA spectra plotted with time (MJD). In the panels we show variations of **a)** disk black-body temperature (T_{in}) in keV, **b)** disk black-body normalization, **c)** power-law (PL) photon index (Γ), and **d)** power-law normalization with time (day). The error bars in the model-fitted components are at 1σ level.

3.3. Spectral energy distribution

We carried out a spectral analysis to study the evolution of the spectral energy distribution during the outburst phase using "standard 2" mode data from the RXTE Proportional Counter Unit 2 (PCU2) in the energy range of 2.5–25 keV. In general, the BH energy spectra (2–25 keV) were modeled by combining the two models *diskbb* and *powerlaw*. The first model was assumed to represent the thermal-component black body, and the later one the non-thermal component, which is mainly due to Comptonized photons. A Gaussian line of peak energy around 6.4 keV (iron-line emission) was used to obtain the best fit. For the spectral fitting, we kept the hydrogen column density (N_H) fixed at 5×10^{21} atoms cm^{-2} (Mendez & van der Klis 1997; Kong et al. 2000; Motta et al. 2009) and also assumed a 0.5% systematic error for the entire spectral fit. We did not include any smeared-edge model component (to account for a reflection component) in our spectral fitting. In this paper, we present the results of the 146 PCA observations spread over the outburst. The best-fit to the energy spectra were obtained by maintaining the value of the reduced χ^2 (χ^2/d.o.f.) of the fit at ~1. After obtaining the best-fit model spectra, we used the "error" command to calculate the error in the fitted parameters. All of these error values are of the 1σ confidence level. We used the "flux LE HE err" command to calculate the errors in the flux for the energy range of LE and HE (in keV).

The daily variations in the fitted model parameters of the 2.5–25 keV RXTE/PCA spectra are plotted in Fig. 7, which clearly reveals the justification of separating the full outburst in

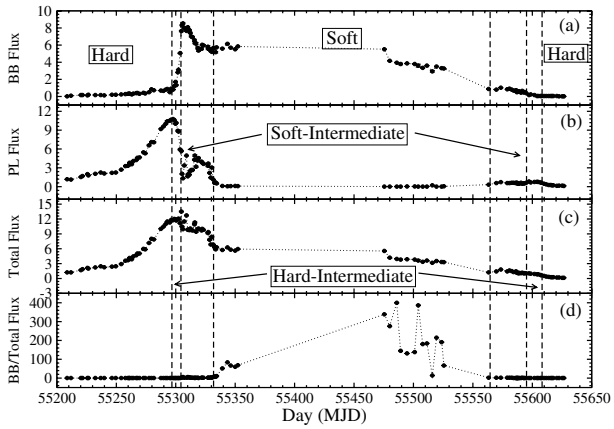

Fig. 8. Derived properties of the daily flux variation. The panels are: **a)** 2.5–25 keV bolometric flux due to the disk black-body component, termed black-body (BB) flux, **b)** 2.5–25 keV flux due to the power-law component, termed power-law (PL) flux, **c)** 2.5–25 keV total flux, and **d)** the ratio of the total to PL fluxes. The error bars of the model fitted fluxes are at 1σ level.

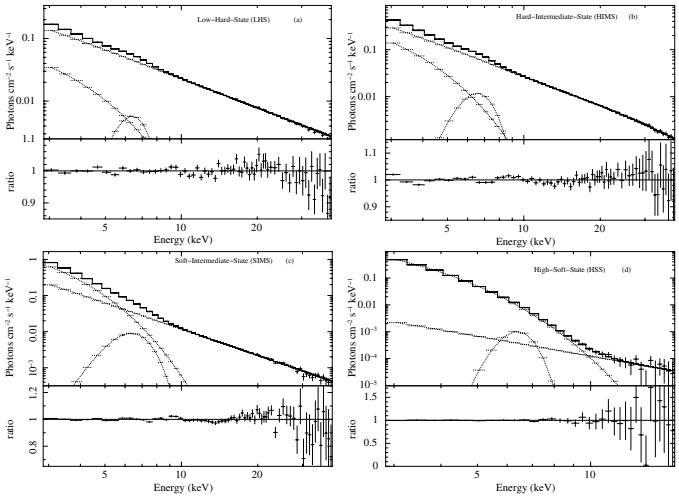

Fig. 9. a–d) 2.5–40 keV (except in **d**, where 2.5–17 keV) RXTE/PCA model fitted spectra with various components from initial four different spectral states are shown. In top left panel **a)** 2010 March 26 (Obs. Id: 95409-01-12-00), a typical hard state spectrum; in top right panel **b)** hard-intermediate state spectrum of 2010 April 13 (Obs. Id: 95409-01-14-06); in bottom left **c)** 2010 April 29 (Obs. Id: 95409-01-16-05), a typical soft-intermediate state spectrum, and in bottom right panel **d)** 2010 September 19 (Obs. Id: 95409-01-35-02), soft state spectrum respectively are shown.

the above-mentioned four states. The panels (a–d) are, respectively, the black body temperature $T_{\rm in}$ in keV, the black body normalization factor, the photon index Γ, and the power-law normalization. Similarly in Fig. 8, the daily variations in the black body (BB) flux (panel a), the power-law (PL) flux (panel b), and the total flux (panel c) are shown. In panel (d), we show how the ratio of the black body to total flux changes daily. The convolution model "cflux" was used to calculate the flux contributions for the thermal (diskbb) and non-thermal (power-law) components for the energy range of 2.5–25 keV.

We note that during the soft spectral state, most of the spectra were fitted up to 10 keV, because of the low and insignificant flux contribution above >∼10 keV (although some of the soft state spectra extends up to ∼15 keV). From the nature of the variations in the power-law indices and disk black-body components, the full outburst is classified in four spectral states with a sequence of *hard* → *hard-intermediate* → *soft-intermediate* → *soft* → *soft-intermediate* → *hard-intermediate* → *hard* states (see, also Fig. 2).

We also analyzed the PCA spectral data up to 40 keV (since the HEXTE spectral data were not useful for such high-energy spectral studies) in a few observations to search for the reflection features, high energy contributions, and particularly the high-energy power-law cutoff in the low-hard states. Hence, we fitted the energy spectra with a phenomenological model (diskbb + power-law), in addition to different combinations of models, such as "smedge", "reflect", and "cutoffpl". We found that hard-state spectra were well-fitted by a phenomenological model without any extra model component, whereas the hard-intermediate state spectra could be fitted with a cut-off power-law (*cutoffpl*) modified by a reflection component (*reflect*) instead of a simple power-law model. An evolution of the high-energy cut-off in the hard states of GX 339-4 was previously reported for the 2006/2007 outburst (Motta et al. 2009). On the other hand, the soft-intermediate state spectra were fitted with the same model combination along with a weak signature of the "smedge" component within the energy range from ∼7 to ∼9 keV, whereas soft-state spectra are well-fitted by a "diskbb" model and a weak power-law component (up to 15 keV).

In Figs. 9a–d, we plot the model-fitted energy spectra (up to 40 keV, except for the soft state up to 17 keV), taken from four different spectral states (see, Fig. 2 labeled a, b, c, and d) of the present outburst of GX 339-4. A detailed modeling of the high energy spectrum in terms of a two component advective flow (TCAF) in different states is beyond the scope of the present work, and will be presented elsewhere. In each spectral plot (top panel), we show the unfolded energy spectrum with its individual model components and in the bottom panel, we show the variation in the ratio (data/model) over the fitted energy range. The best-fit model parameters for different states of the outburst are presented in Table 2.

Table 2. PCA spectral model fitted parameters.

Obs.	Diskbb $T_{\rm in}$(keV)	Diskbb Norm.	PL Index(Γ)	PL Norm.	BB Flux	PL Flux	χ^2/d.o.f.
(1)	(2)	(3)	(4)	(5)	(6)	(7)	(8)
26	$1.304^{+0.041}_{-0.031}$	$17.66^{+1.580}_{-0.840}$	$1.549^{+0.016}_{-0.016}$	$0.808^{+0.015}_{-0.019}$	$0.524^{+0.045}_{-0.049}$	$10.36^{+0.065}_{-0.066}$	76.52/60
35	$1.012^{+0.044}_{-0.041}$	$207.9^{+5.500}_{-8.700}$	$2.024^{+0.062}_{-0.062}$	$3.062^{+0.087}_{-0.156}$	$1.651^{+0.118}_{-0.127}$	$10.18^{+0.306}_{-0.316}$	77.59/60
51	$0.878^{+0.009}_{-0.009}$	$1820^{+35.00}_{-37.00}$	$2.425^{+0.022}_{-0.022}$	$3.139^{+0.184}_{-0.173}$	$6.551^{+0.041}_{-0.041}$	$5.547^{+0.036}_{-0.036}$	95.26/61
141	$0.735^{+0.007}_{-0.005}$	$3557^{+101.0}_{-95.00}$	$2.444^{+0.025}_{-0.041}$	$0.034^{+0.002}_{-0.005}$	$4.462^{+0.019}_{-0.019}$	$0.048^{+0.015}_{-0.022}$	14.43/28
208	$0.663^{+0.015}_{-0.016}$	$1081^{+58.00}_{-49.00}$	$2.344^{+0.085}_{-0.085}$	$0.343^{+0.021}_{-0.026}$	$0.706^{+0.016}_{-0.016}$	$0.719^{+0.013}_{-0.013}$	80.42/61
222	$1.065^{+0.037}_{-0.046}$	$15.99^{+0.280}_{-1.940}$	$1.661^{+0.044}_{-0.032}$	$0.096^{+0.005}_{-0.006}$	$0.166^{+0.010}_{-0.011}$	$0.966^{+0.008}_{-0.008}$	54.67/61
226	$1.100^{+0.034}_{-0.011}$	$4.040^{+0.254}_{-0.197}$	$1.462^{+0.023}_{-0.024}$	$0.049^{+0.010}_{-0.009}$	$0.049^{+0.009}_{-0.010}$	$0.829^{+0.009}_{-0.009}$	42.47/62

PCA spectral fluxes are calculated in 2.5–40 keV energy range (except 2.5–17 keV for soft state (Obs. = 141) spectrum) and photon fluxes in units of 10^{-9} erg cm^{-2} s^{-1}.

3.4. Physical modeling of q-diagram with a two-component flow

The HID of the outburst profile of GX 339-4 can be explained by a two-component advective flow (TCAF) model. An outburst is a time-dependent phenomenon, hence it can be analyzed completely by a steady-state model. We followed the prescription given in Mandal & Chakrabarti (2010) to fit the main features of the HID of GX 339-4. The outburst might have been triggered by a sudden change in the viscosity that caused a conversion

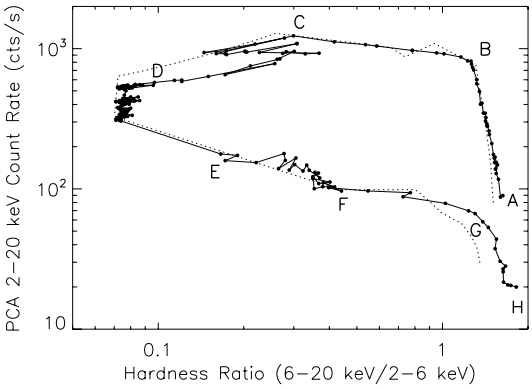

Fig. 10. Two component accretion flow model fitted (dotted curve) HID of GX 339-4 during the 2010-11 outburst. The solid curve with points show the observed data as shown in Fig. 2 and indicators $A - H$ are also have the same meanings.

of sub-Keplerian into Keplerian matter. This increase in the Keplerian rate, along with the inward movement of the shock front (as suggested by the evolution of the QPOs) explains the outburst profile. In the rising phase, a high sub-Keplerian rate makes the spectrum hard and a smooth increase in Keplerian rate increases the total photon counts. The source GX 339-4 moved to an intermediate/soft state when the Keplerian rate was sufficiently high and the sub-Keplerian rate decreased to a low value such that the supply of soft photons was sufficient to cool the hot electrons in the post-shock region. Finally, in the decline phase, the Keplerian rate decreased and the sub-Keplerian rate approached the value at the quiescent state before the spectral state became hard again. In Fig. 10, the solid line with points shows the observed data, while the dotted line represents the model fit. We started the fitting process from the day that the QPO first appeared (22 March, 2010). In the rising phase (t_r), the Keplerian rate increased with power-law index (α_d), the shock started to propagate inward with a constant velocity (v_0), and sub-Keplerian rate remains almost constant (B_f). The sub-Keplerian matter decreased with a power-law index (α_{h1}) between (t_r) and (t_h) and then started to increase. While the Keplerian rate decreased very slowly (linearly with a slope 0.0035 Eddington rate/day) after t_d until t_h, and then as a power-law (α_d) with time. The shock started to recede outward after t_s. The slow decrease in Keplerian rate (from t_d to t_h) kept the source in a very soft state for over 217 days. This behavior of GX 339-4 is surprisingly different from GRO J1655-40 where Keplerian rate decreases by a constant power-law. The fit between "$C-D$" in Fig. 10 differs from the observed data since the result is very sensitive to the time variation in the parameters caused by the large number of soft photons in comparison with the hot electrons. In the decline phase, the sub-Keplerian rate in our model increases following a single power-law index but one may need to vary the power-law index to fit the data in the interval "$F-H$". The parameters for the present fit are given in Table 3. The most important point is that the accretion-rate variation does not retrace its path when returning to quiescence, owing to the hysteresis behavior. For more detailed relations among the parameters, we refer to Mandal & Chakrabarti (2010).

4. Discussion and concluding remarks

As a very enigmatic transient X-ray BH candidate, GX 339-4 has underwent several X-ray outbursts after its discovery in the early 1970s. The detailed timing and spectral analysis results

Table 3. Parameters for Fig. 10.

t_r	t_d	t_h	t_s	α_d	α_{h1}	Xs_o	Xs_i	v_0	B_f
Time(day)						(r_g)	(r_g)	(r_g/day)	
19.0	30.0	247.0	325.0	−1.0	−0.6	400	14.0	12.8	2.0

using RXTE/PCA instrument that we have presented in this paper reveal several very important aspects about the nature of the transient accretion process around a black hole. From the nature of the variations in the light curves, color-color variations, power spectra, energy spectra, and most importantly the variation in the QPO frequency, one can develop a comprehensive picture of what might be happening when such an outburst takes place.

The most natural assumption about the cause of the outburst is the change in the physical properties of the matter such as viscosity, perhaps owing to the enhanced magnetic activity. During the rising phase of the outburst, the viscosity may cause an increase in the accretion rate of the Keplerian matter. The outburst phase then subsides with the drop in viscosity and the Keplerian rate is reduced and the disk itself recedes. According to the two-component advective flow (TCAF) model (Chakrabarti 1990; Chakrabarti & Titarchuk 1995), the initial phase is dominated by a low angular-momentum sub-Keplerian flow and the spectrum is found to be in a hard/low-hard state. As the outburst progresses, and the accretion rate in the Keplerian component increases and the object enters a soft spectral state. Finally, during the declining phase of the outburst, the Keplerian flow recedes while the sub-Keplerian matter rate remains roughly the same, which makes the spectrum harder. Debnath et al. (2008) found that this picture explains the 2005 GRO J1655-40 outburst quite successfully. From Figs. 7 and 8, one can also see that the above-mentioned picture is relevant to the recent GX 339-4 outburst, although the rate variation is not time-symmetric with respect to the peak. This causes the hysteresis loop behavior or the so-called "q"-diagram.

It is clear from Fig. 1a that during the hard and hard-intermediate states of the rising phase of the outburst, 2–20 keV photon count rate increases initially slowly (in the hard state), then rapidly (in the hard-intermediate state). In addition, from the hardness ratio plot of Fig. 1, one can note that the hardness ratios of the 6–20 to 2–6 keV photon rates initially decrease slowly (in the hard state) and then rapidly (in the hard-intermediate state). During both of these states, the low-energy disk black-body flux increases, whereas the high-energy power-law flux increases slowly in the hard state and rapidly decreases during the hard-intermediate state. During the hard state, the disk temperature (T_{in}) is ∼1.5 keV, whereas during the hard-intermediate state its value decreases to ∼0.9 keV (see Fig. 7) within ∼9 days. This is because during the hard spectral states both the high-energy and low-energy flux increase at almost the same rate (see, Fig. 8), whereas during the hard-intermediate state the high energy flux decreases owing to the decrease in the sub-Keplerian rate but the Keplerian rate remains almost constant. As a result, the disk becomes cool and its temperature decreases sharply. Furthermore, during the hard spectral state, the power-law photon index (Γ) increases slowly from ∼1.3 to ∼1.7, within a period of about three months, whereas during the hard-intermediate state, which has a period of ∼9 days, it rapidly increases to ∼2.3. This is because during the hard state, the spectra are dominated by the sub-Keplerian flow. As the day progresses, the Keplerian rate increases slowly in the hard state and rapidly in the hard-intermediate state, owing to the low-angular

momentum sub-Keplerian flow moving on an infall timescale as the Keplerian flow moves towards the black hole on a viscous timescale.

The number of soft photons becomes comparable to those of hot electrons during the soft-intermediate spectral state. As a result, during this state the photon index became constant with $\Gamma \sim 2.4$. The spectra were then subsequently dominated by the Keplerian flow with a decrease in the sub-Keplerian flow and the spectrum becoming softer. As a result, the photon index increases further, becoming >3.0. During the soft spectral state, the hard X-ray photon flux above ∼15 keV, decreased rapidly, i.e., we can conclude that during this phase of the outburst, the inverse Comptonized sub-Keplerian flow decreases rapidly and the spectra are dominated by thermal Keplerian cool photons. Hence during the soft-state, the disk temperature ($T_{\rm in}$) was observed to be <0.7 keV, whereas in the previous soft-intermediate spectral state it had been observed to be constant at ∼0.9 keV.

After spending about seven months in the Keplerian-flow-dominated soft spectral state, the source returned to a soft-intermediate spectral state. During this declining phase of the outburst, nearly identical behavior was observed as in the rising soft-intermediate spectral state. During this spectral state, Γ was observed to be ∼2.3–2.5 with $T_{\rm in}$ at ∼0.6 keV, owing to the slow increase of the sub-Keplerian component. The source then moved to a declining hard-intermediate spectral state with rapidly decreasing Γ from 2.3 (of the previous state) to ∼1.6 and increasing $T_{\rm in}$ from the previous state value of ∼0.6 keV to ∼1.27 keV within a few days. The physical reason for this is the deficiency of the fresh supply of Keplerian matter as the viscosity is reduced. Thus, on the whole, the fraction of Keplerian cold matter decreases, whereas the sub-Keplerian matter increases making the disk become hotter and causing the source to move to a hard spectral state. Here the power-law photon index Γ is observed to decrease to ∼1.3 from its previous state value of ∼1.6 and its disk black-body temperature $T_{\rm in}$ is increased to ∼1.8, from its previous state value of ∼1.27 keV.

During the rising phase of the outburst, strong QPOs were observed and in both the hard and hard-intermediate states the QPO frequencies increased monotonically with time. The formation of strong QPOs and the smooth variation in QPO frequencies during this phase (Debnath et al. 2010) indicates that the physical processes behind the formation of QPOs are identical each day and related to the dynamics of the infalling matter. We decided to choose the shock oscillation model (SOM) solution inside a sub-Keplerian disk, which has been demonstrated to have a stable oscillation for many dynamical timescales (Molteni et al. 1996; Ryu et al. 1997; Chakrabarti & Manickam 2000; Chakrabarti et al. 2004, 2005, 2008, 2009; Debnath et al. 2010, 2012). In this SOM solution, at the rising phase of the outburst, a shock wave moves toward the black hole, which oscillates either because of a resonance (where the cooling time of the flow is approximately the infall time; Molteni et al. 1996) or because the Rankine-Hugoniot condition is not satisfied (Ryu et al. 1997) to form a steady shock. In the propagating oscillatory shock (POS) model, which is the propagatory case of SOM, it is easy to verify that the QPO frequencies (which are the inverses of the infall times from the post-shock to the BH) are simply related to the drifting of the shock towards (rising phase) or away from (declining phase) the BH. Debnath et al. (2010) inferred the movement of the shock wave towards BH for the same GX 339-4 outburst with a constant velocity of ∼10 m s^{-1}. Similar movements of shock waves (∼20 m s^{-1}) were observed by Chakrabarti et al. (2008, 2009) during the rising phases of GRO J1655-40 and XTE J1550-564. In the declining phase, Chakrabarti et al. (2008, 2009) observed that the shock waves receded from the BH. During the declining soft-intermediate spectral state of the outburst, QPOs are observed sporadically on and off at a frequency ∼2 Hz for around ∼29 days. After that, during the declining hard-intermediate spectral state, the QPO frequencies are observed to decrease monotonically from 6.42 Hz to 1.149 Hz within a period of ∼10 days. The QPO evolution during this phase is also fitted by the same POS model solution, the evolutions being more or less same as that of the declining phase of 2005 GRO J1655-40 outburst (Chakrabarti et al. 2008), in which the evolution of the decline phase had two parts. Then in the initial 3.5 days, the shock moved away from the BH slowly and then rapidly. Here we also discern two behaviors. Initial 4.2 days, the shock is found to move slowly (with an acceleration of 20 cm s^{-1} day^{-1}). Subsequently, it moves with a higher rate of acceleration (175 cm s^{-1} day^{-1}). During this period, the shock velocity varies from 205 cm s^{-1} to 1785 cm s^{-1} with an intermediate value of 288 cm s^{-1} on the 4.2nd day. At the same time, the shock is also found to move away from the BH from 84 $r_{\rm g}$ to 751 $r_{\rm g}$ passing via an intermediate location of 155 $r_{\rm g}$ on the transition (4.2nd) day. The universality of the behavior leads us to believe that the same processes are in operation in all the outbursting sources. However, an understanding of the details, such as the cause of the break in the QPO evolution during the declining phase, is still missing.

We have been able to model the evolution of power spectra in different spectral states with different combinations of Lorentzian and power-law like profiles, hence found that it can be explained with the diffusive propagation of perturbation in two different accretion flows (CT95, TSA07). The observed rms power decreases as the source moves from a hard-state to a soft-state, which is also quite natural in most outburst sources. The evolution pattern (i.e., q-diagram), which is characteristic of the outburst sources, of the 2010-11 outburst of GX 339-4 is modeled and explained with the two component advective flow (TCAF) model very successfully.

The interpretation of the disk-jet dynamics in outburst BH sources has proven to be another challenging task. Several quasi-simultaneous observations of GX 339-4 in multi-wavelength studies (Homan et al. 2005; Markoff et al. 2005; Maitra et al. 2009; Coriat et al. 2009) strongly suggest that the radio jets are associated with the hard state of the source and also illustrates the compact nature of the jet. The broadband continuum (radio through to X-rays) of GX 339-4 was described by a jet-dominated model (see, Markoff et al. 2005; Maitra et al. 2009), in which the base of the jet was considered to be the hard X-ray emitting region. In reality, the base is nothing but the post-shock region, known as the CENBOL (i.e., the CENtrifugal pressure-dominated BOundary Layer) of TCAF, as the base of the jet, is able to explain the broadband nature of the spectrum. The broadband spectra of M 87 (Mandal & Chakrabarti 2008) has been explained with TCAF model and the modeling of the multi-wavelength nature of the spectrum of GX 399-4 will be presented elsewhere. Since the basic cause of the outburst is believed to be the enhancement of viscous processes, simultaneous radio observations or the observations of the companion during the onset could provide valuable information about the outbursting properties. ASTROSAT, India's upcoming multi-wavelength Satellite, will possibly shed light on the "basic cause" of the outburst, as it carries instruments to study both the ultraviolet (observing the outer parts of the disk) and X-ray (observation of the inner parts of the disk) emission from the outbursting systems.

Acknowledgements. We thank the anonymous referee for the detailed comments and suggestions to improve the quality of the manuscript.

References

Belloni, T., & Hasinger, G. 1990, A&A, 230, 103
Belloni, T., Colombo, A. P., Homan, J., et al. 2002a, A&A, 390, 199
Belloni, T., Psaltis, D., & van der Klis, M. 2002b, ApJ, 572, 392
Belloni, T., Homan, J., Casella, P., et al. 2005, A&A, 440, 207
Chakrabarti, S. K. 1990, Theory of Transonic Astrophysical Flows (Singapore: World Scientific)
Chakrabarti, S. K., & Titarchuk, L. G. 1995, ApJ, 455, 623 (CT95)
Chakrabarti, S. K., & Manickam, S. G. 2000, ApJ, 531, L41
Chakrabarti, S. K., Acharyya, K., & Molteni, D. 2004, A&A, 421, 1
Chakrabarti, S. K., Nandi, A., Debnath, D., et al. 2005, IJP, 79, 841
Chakrabarti, S. K., Debnath, D., Nandi, A., et al. 2008, A&A, 489, L41
Chakrabarti, S. K., Dutta, B. G., & Pal, P. S. 2009, MNRAS, 394, 1463
Chen, W., Shrader, C. R., & Linio, M. 1997, ApJ, 491, 312
Coriat, M., Corbel, S., Buxton, M. M., et al. 2009, MNRAS, 400, 123
Cowley, A. P., Schmidtke, P. C., Hutchings, J. B., et al. 2002, ApJ, 123, 1741
Debnath, D., Chakrabarti, S. K., Nandi, A., et al. 2008, BASI, 36, 151
Debnath, D., Chakrabarti, S. K., & Nandi, A. 2010, A&A, 520, 98 (Paper I)
Debnath, D., Chakrabarti, S. K., & Nandi, A. 2012, New Astron., submitted
Dunn, R. J. H., Fender, R. P., Körding, E. G., et al. 2010, MNRAS, 403, 61
Frank, J., King, A. R., & Raine, D. J. 2002, Accretion Power in Astrophysics, 3rd edition (Cambridge University Press)
Homan, J., & Belloni, T. 2005, Ap&SS, 300, 107
Homan, J., Wijnands, R., van der Klis, M., et al. 2001, ApJS, 132, 377
Hynes, R. I., Steeghs, D., Casares, J., et al. 2003, ApJ, 583, L95
Hynes, R. I., Steeghs, D., Casares, J., et al. 2004, ApJ, 609, 317
Ilovaisky, S. A., Chevalier, C., Motch, C., et al. 1986, A&A, 164, 671
Jahoda, K., Swank, J. H., Giles, A. B., et al. 1996, Proc. SPIE, 2808, 59
Kong, A. K. H., Kuulkers, E., Charles, P. A., et al. 2000, MNRAS, 312, L49
Körding, E., Rupen, M., Knigge, C., et al. 2008, Science, 320, 1318
Maccarone, T. J., & Coppi, P. S. 2003, MNRAS, 338, 189
Maejima, Y., Makishima, K., Matsuoka, M., et al. 1984, ApJ, 285, 712
Mandal, S., & Chakrabarti, S. K. 2008, ApJ, 689, L17
Mandal, S., & Chakrabarti, S. K. 2010, ApJ, 710, L147
Maitra, D., Markoff, S., Brocksopp, C., et al. 2009, MNRAS, 398, 1638
Markert, T. H., Canizares, C. R., Clark, G. W., et al. 1973, ApJ, 184, L67
Markoff, S., Nowak, M. A., & Wilms, J. 2005, ApJ, 635, 1203
McClintock, J. E., & Remillard, R. A. 2006, in Compact stellar X-ray sources, ed. W. Lewin, & M. van der Klis, Cambridge Astrophys. Ser., 39 (Cambridge, UK: Cambridge University Press) [arXiv:astro-ph/0306213]
Mendez, M., & van der Klis, M. 1997, ApJ, 479, 926
Miller, J. M., Fabian, A. C., Reynolds, C. S., et al. 2004, ApJ, 606, L131
Miyamoto, S., Kimura, K., Kitamoto, S., et al. 1991, ApJ, 383, 784
Molteni, D., Sponholz, H., & Chakrabarti, S. K. 1996, ApJ, 457, 805
Motta, S., Belloni, T., & Homan, J. 2009, MNRAS, 400, 1603
Nowak, M. A., Wilms, J., & Dove, J. B. 1999, ApJ, 517, 355
Nowak, M. A. 2000, MNRAS, 318, 361
Remillard, R. A., & McClintock, J. E. 2006, ARA&A, 44, 49
Remillard, R. A., Morgan, E. H., McClintock, J. E., et al. 1999, ApJ, 522, 397
Remillard, R. A., Sobczak, G. J., Muno, M. P., et al. 2002, ApJ, 564, 962
Ryu, D., Chakrabarti, S. K., & Molteni, D. 1997, ApJ, 474, 378
Shakura, N. I., & Sunyaev, R. A. 1973, A&A, 24, 337
Titarchuk, L., Shaposhnikov, N., & Arefiev, V. 2007, ApJ, 660, 556 (TSA07)
Tomsick, J. A. 2010, ATel, 2384, 1
van der Klis, M. 2005, AN, 326, 798
Wijnands, R., Homan, J., & van der Klis, M. 1999, ApJ, 526, L33
Yamaoka, K., Nakahira, S., Mihara, T., et al. 2010, ATel, 2380, 1
Zdziarski, A. A., Gierliński, M., Mikolajewska, J., et al. 2004, MNRAS, 351, 791